EXPERIMENTAL PERFORMANCE OF A COMBINED THROTTLING DEVICE WITH STEPPER MOTOR AND NEEDLE VALVE IN AN AMMONIA-WATER ABSORPTION REFRIGERATION SYSTEM

XingYuan HUO[a], XiaoLin SUN[a,b,c*], JinFeng WANG[a,b,c*], JianGuo ZHANG[d], ZhiGang ZHOU[d], Yu HU[d]

[*a] Department of Refrigeration and Air Conditioning Engineering, Shanghai Ocean University, Shanghai, China

[b] Shanghai Professional Technology Service Platform on Cold Chain Equipment Performance and Energy Saving Evaluation, Shanghai, China

[c] Shanghai Experimental Teaching Demonstration Center for Refrigeration and Air Conditioning Engineering, Shanghai Ocean University, Shanghai, China

[d] CEGT (Shanghai) Technology Co., Ltd., Shanghai, China

[*] Corresponding author; E-mail: xlsun@shou.edu.cn; jfwang@shou.edu.cn

Electronic expansion valves (EEVs) for ammonia-water absorption refrigeration systems are expensive and limited in model selection. In this paper, a combined throttling device (CTD) based on a stepper motor and needle valve is proposed to replace the electronic expansion valve (EEV). An experimental platform was established to study its performance. Results show that with PID, fuzzy, and fuzzy PID superheat degree control algorithms, the maximum deviation of the superheat degree is no more than 1 ° C, and fuzzy PID reduces fluctuation by 14.6% at the superheat degree of 9.5 ° C compared with PID. At the superheat degree of 9.5 ° C, the system performs refrigerating capacity of 2.8kW and COP of 0.48. The experimental results validate the practical feasibility and engineering application potential of the proposed CTD for ammonia-water absorption refrigeration systems.

Key words*: ammonia-water absorption refrigeration, combined throttling device, superheat degree, control algorithms, fuzzy PID*

1.Introduction

Absorption refrigeration system is a type of thermal-powered system, which offers advantages over compression systems including environmental friendliness and the ability to harness low-grade heat[1, 2]. In both vapor compression and absorption refrigeration systems, precise and stable control of the superheat degree is essential for improving the system efficiency and ensuring the safe, reliable operation of the equipment[3], Thermal expansion valve (TEV) and electronic expansion valve (EEV) are used a lot for superheat degree

control[4]. At the same time, research focuses on the control of superheat degree for absorption refrigeration system are not as common as those for compression refrigeration system.

Yuqi Shi[5] proposed a novel generator-absorber exchange(GAX) absorption refrigeration cycle incorporating two TEVs within the system. Results demonstrated that COP of this cycle is 20% higher than that of the standard GAX (SGAX) cycle. Dandan Zhao[6] investigated the performance of an air-cooled lithium bromide absorption refrigeration system using a thermal expansion valve(TEV). M. Yari[7]proposed three thermal-driven chillers comprising absorption refrigeration and a transcritical CO_2 cascade cycle with jet throttling. An EEV was employed in this system. M. Imroz Sohel[8] proposed a novel dynamic simulation approach for gravity-assisted solution pumps in ammonia absorption refrigeration units. By employing a float-regulated expansion valve the influences of varying pump design parameters on flow rate were investigated. Matthew Elliott[9] proposed a hybrid expansion valve (HEV) and compared the performance of the HEV system with the performances of the TEV and EEV systems. Additionally, existing research explores various control algorithms and strategies for superheat degree regulation, including dual-loop model-free adaptive iterative learning control, MIMO control based on evaporator two-phase length and superheat degree, and improved traditional control schemes, such as fractional order PID control optimized by algorithms, self-tuning fuzzy logic control, adaptive PID control, adaptive-model predictive control, and semi-active flow control emulation[10–16].

Thermal expansion valves (TEVs) are widely used in refrigeration systems but suffer from drawbacks such as slow response and limited adjustment range, and a potential alternative is the EEV. However, in absorption refrigeration systems, available EEV models are limited, and the procurement costs are very high.

In this study, a combined throttling device (CTD) composed of a stepper motor and a needle valve is proposed to replace the EEV, at a cost of only 1/8 of the EEV. An ammonia-water absorption refrigeration system is established for experimental investigation on the performance of this device.

2. Introduction to the ammonia-water absorption refrigeration experimental platform

2.1 Principles and equipment of the ammonia-water absorption refrigeration experimental platform

The experimental study was conducted on an ammonia-water absorption refrigeration system, as shown in Fig.1. The system operates under the following typical working conditions: generator temperature of 110 °C~140 °C, hot oil temperature of 130 °C~150 °C, absorber feed flow rate of 48kgh^{-1}~78kgh^{-1}, distillation column feed flow rate of 53kgh^{-1}~89kgh^{-1}, low-side pressure of 2bar~5bar, high-side pressure of 10bar~20bar, and absorber temperature of 30 °C~55 °C. The degassing rate of the system is determined to be in the range of 0.12~0.17, which is calculated based on the generation temperature, absorber temperature, low-side pressure, and high-side pressure. The rated refrigerating capacity of the system is 3 kW. Fig. 2 illustrates the schematics of the system. The key components of the system consist of a generator, distillation column, condenser, subcooler, throttling device (CTD), evaporator, absorber, and solution heat exchanger. The refrigeration cycle consists of four fundamental processes: generation, condensation, evaporation, and absorption[17].

The fundamental operating mechanism of ammonia-water absorption refrigeration has been clearly elaborated in previous studies[18]. In this paper, the absorption refrigeration system is powered by thermal energy, which is provided to the generator by hot oil. The ammonia solution is heated within the generator, and the desorbed ammonia vapor passes through the stripping section, the rectification section, and the reflux section of the distillation column to yield pure ammonia vapor. The ammonia vapor then condenses to liquid in the condenser. After throttling, the low-temperature working fluid evaporates in the evaporator, absorbing heat from the chilled water. In the absorber, the dilute solution from the generator absorbs ammonia vapor to become the concentrated solution, which is then pumped back to the generator. A solution heat exchanger installed between these two components recovers heat to improve system efficiency. Table 1 summarizes the parameters of the principal components.

The Equation. (1) is the generator heat input.

$$Q_G = c_{oil}\dot{m}_{oil}\left(T_{oil,in} - T_{oil,out}\right) \quad (1)$$

Where Q_G[kW], c_{oil}[KJ Kg^{-1} K^{-1}], $\dot{m}_{oil}$[kgh^{-1}], $T_{oil,in}$[℃], $T_{oil,out}$[℃] are the heat input of the generator, specific heat of the hot oil, mass flow rate of the hot oil, inlet temperature of the hot oil, and outlet temperature of the hot oil.

The Equation. (2) is the heat exchanging capacity of the condenser.

$$Q_C = c_w\dot{m}_{cow1}\left(T_{cow1,out} - T_{cow1,in}\right) \quad (2)$$

Where Q_C[kW], c_w[KJ Kg^{-1} K^{-1}], $\dot{m}_{cow1}$[kgh^{-1}], $T_{cow1,in}$[℃], $T_{cow1,out}$[℃] are the heat exchanging capacity of the condenser, specific heat of water, mass flow rate of the condenser cooling water, inlet temperature of the condenser cooling water, and outlet temperature of the condenser cooling water.

The Equation. (3) is the heat exchanging capacity of the absorber.

$$Q_A = c_w\dot{m}_{cow2}\left(T_{cow2,out} - T_{cow2,in}\right) \quad (3)$$

Where Q_A[kW], $\dot{m}_{cow2}$[kgh^{-1}], $T_{cow2,in}$[℃], $T_{cow2,out}$[℃] are the heat exchanging capacity of the absorber, mass flow rate of the absorber cooling water, inlet temperature of the absorber cooling water, and outlet temperature of the cooling water.

The Equation. (4) is the refrigerating capacity of the system.

$$Q_R = c_w\dot{m}_{chw}\left(T_{chw,in} - T_{chw,out}\right) \quad (4)$$

Where Q_R[kW], $\dot{m}_{chw}$[kgh^{-1}], $T_{chw,in}$[℃], $T_{chw,out}$[℃] are the refrigerating capacity of the system, mass flow rate of the chilled water, inlet temperature of the chilled water, and outlet temperature of the chilled water.

The Equation. (5) is the coefficient of performance (COP) of the system.

$$COP = Q_R/Q_G \quad (5)$$

The total power of the pumps is much lower than Q_G (the generator heat input), thus, only Q_G is considered when calculating the COP.

Fig.1. Ammonia-water absorption refrigeration experimental platform

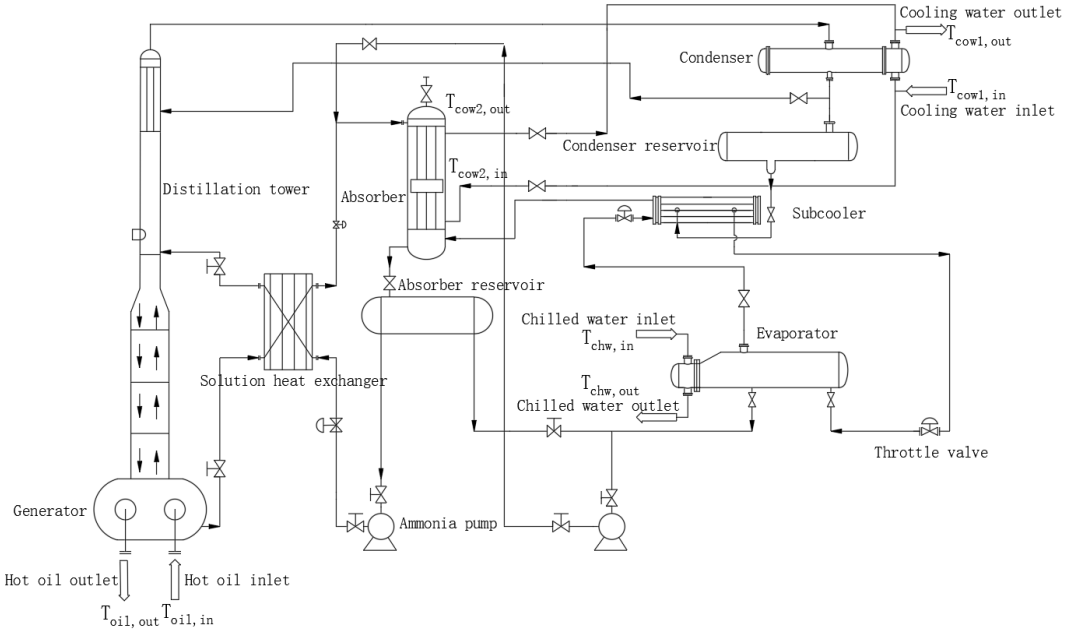

Fig.2. Schematics of the ammonia-water absorption refrigeration experimental platform

Table 1. Ammonia-water absorption refrigeration system equipment parameters

Name	Model	Specifications
Solution heat exchanger	HZL26R-18D	Heat transfer area: 0.416m^2
Condenser	HZL26R-24D	Heat transfer area: 0.572m^2
Evaporator	HZL95BR-46X	Heat transfer area: 4.18m^2
Needle valve	Swagelok SS-ORS2	Throat diameter:0.08in
Stepper motor	Lei Sai -57CM13	Rated current：4A
Stepper motor driver	DM542J	Pulse voltage:5V-24V Rated current：4.2A
Electronic expansion valve	Danfoss AKVA10-1	Rated capacity:4kW

Due to inherent measurement errors in the sensors, uncertainty analysis calculations are also performed to determine the accuracy in sensors, Q_R, Q_G, and COP. The results are presented in Table 2.

Table 2. Accuracy and uncertainty analysis

Name	Accuracy
Temperature sensor	± 0.5%
Pressure sensor	± 0.5%
Cooling water flow meter	± 0.5%
Chilled water flow meter	± 0.5%
Hot oil flow meter	± 0.5%
Ammonia solution flow meter	± 0.5%
Q_R	±1.0%
Q_G	±1.0%
COP	±2.0%

2.2 Control logic of the experimental platform

As depicted in Fig. 3, the control system for the experimental platform comprises PLC: a data acquisition module, a control module, and an execution module. The PLC receives signals from the acquisition module and sends processed commands to the execution module. Communication between the PLC and the touchscreen is achieved via PROFINET. The platform control logic is illustrated in Fig. 4.

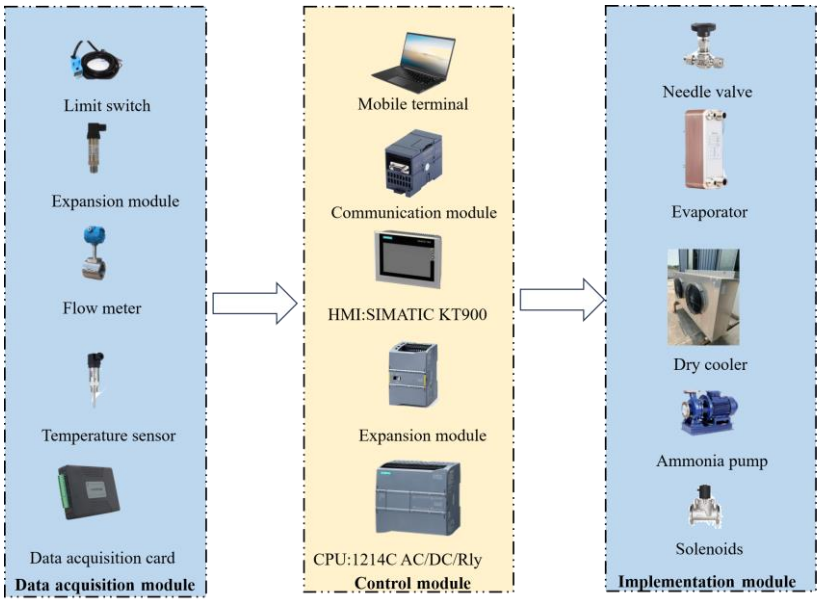

Fig.3. Schematics of the control system for the experimental platform

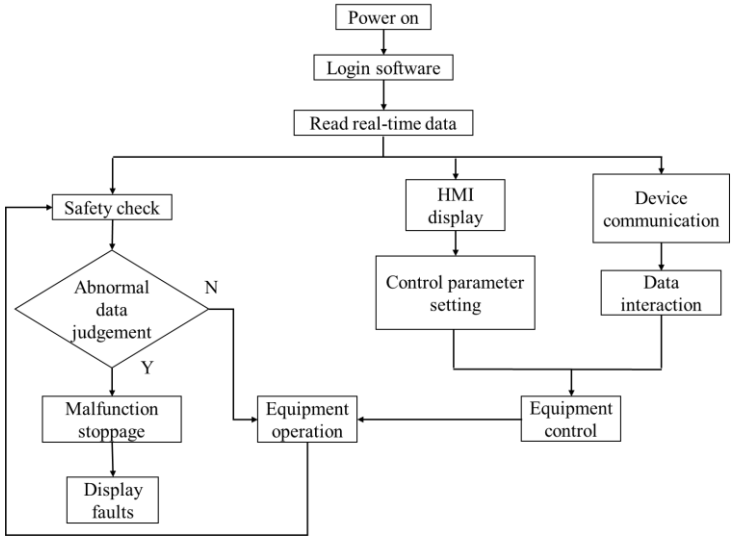

Fig.4. Control logic for the experimental platform

2.3 The CTD and the control system

In this study, a CTD based on a stepper motor-driven needle valve is proposed as a alternative to EEV, and the CTD control system based on the PLC and LabVIEW platforms is also developed.

The CTD drives the motor via a stepper motor driver, thereby rotating the needle valve stem to achieve valve opening adjustment. A pair of limiting devices are incorporated to protect the valve from damage caused by stepper motor overshoot. The schematics of the throttling assembly and signal board is depicted in Fig. 5. The flow coefficient of the adopted needle valve is linearly proportional to the number of steps of the stepper motor, and the variation of the flow coefficient with steps is plotted in Fig. 6.

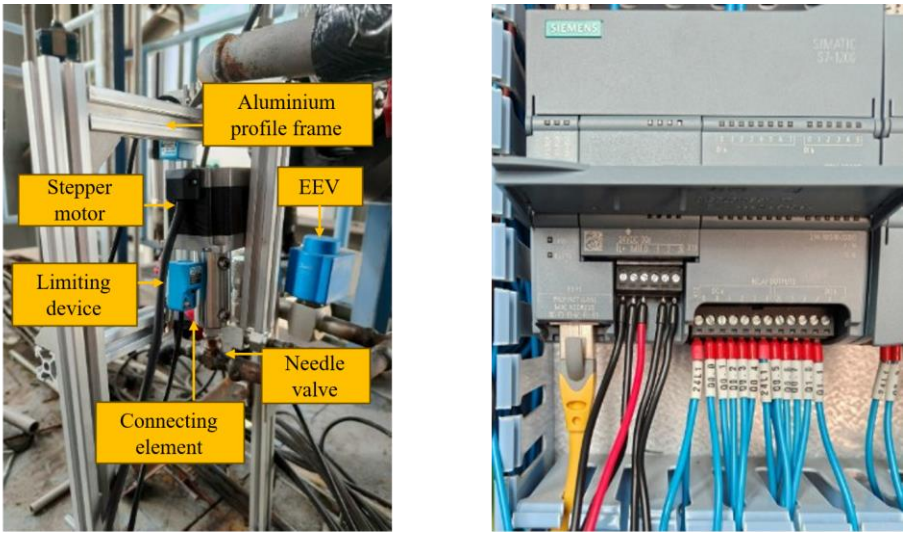

(a) Needle valve with stepper motor control unit (b) Signal board

Fig.5. CTD and signal board

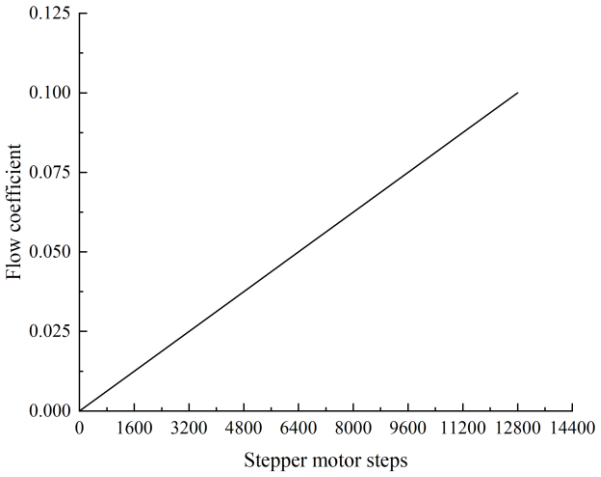

Fig.6. Flow coefficient versus stepper motor steps

A PLC-based stepping motor system receives valve angle and speed commands from LabVIEW. The PLC outputs pulse signals to the driver to regulate the needle valve opening dynamically. The PLC program is developed by configuring control parameters and implementing four main modules: startup, relative displacement, pause, and reset. In this study, more intricate control functions, such as stepper motor operation and superheat degree control algorithms, are implemented in the LabVIEW program.

The LabVIEW control program is primarily responsible for real-time acquisition of evaporator outlet pressure and temperature, deriving the corresponding saturation temperature, calculating the deviation of the superheat degree, deviation change rate of the superheat degree, determining valve opening magnitude, and assessing valve opening direction.

By combining the dedicated PLC program with the LabVIEW program, the CTD could perform fast dynamic response, and microstepping of the motor is conducted to ensure the control precision, making the CTD a suitable substitute to EEV.

Based on these control principles, a corresponding LabVIEW control program was designed.

3. Experimental investigation on superheat degree control

Three types of superheat degree control algorithms were tested: Proportional Integral Derivative (PID) control, fuzzy control, and fuzzy PID control. Input/output parameters of the three control algorithms are as shown in Table 3.

Decreased superheat degree can enhance system efficiency, but stable control at low superheat degree remains challenging. As expansion valve opening enlarged, when superheat degree is low, alternation between superheated vapor and two-phase flow at the evaporator outlet, causing periodic fluctuations in evaporation temperature and superheat degree [17]. So stable control at a low superheat degree is difficult to achieve.

Furthermore, in order to guarantee sufficient heat transfer and eliminate the risk of liquid refrigerant carryover to the absorber, the area of the evaporator was actually larger than needed in this study, leading to a high superheat degree. Accordingly, the minimum superheat degree for this experiment is set at 9.5°C.

Table 3. Control strategy input/output parameters

Control strategy	Controller input	Controller output
PID	e e_c Proportional coefficient K_p Integral coefficient K_i Derivative coefficient K_d	Throttle device opening adjustment amount
Fuzzy	e e_c	Throttle device opening adjustment amount
Fuzzy PID	e e_c Proportional coefficient K_p Integral coefficient K_i Derivative coefficient K_d	Proportional gain ΔK_p Integral gain ΔK_i Derivative gain ΔK_d Throttle device opening adjustment amount

PID is one of the most commonly used control algorithms of electronic expansion valve[19], the PID control algorithm comprises three components: proportional, integral, and derivative. The fundamental PID formula is as shown in Equation. (6).

$$U(t) = K_p e(t) + K_i \int_0^t e(t)dt + K_d \frac{de(t)}{dt} \tag{6}$$

Where $e(t)$, $U(t)$, K_p, K_i, K_d are the error signal, output signal, proportional coefficient, integral coefficient, derivative coefficient.

The PID controller input parameters are e (deviation of the superheat degree), e_c (deviation change rate of the superheat degree), K_p, K_i, and K_d. The output is the throttle device opening adjustment amount. The parameters are determined by the Ziegler-Nichols method. The principle of the PID controller is illustrated in Fig. 7.

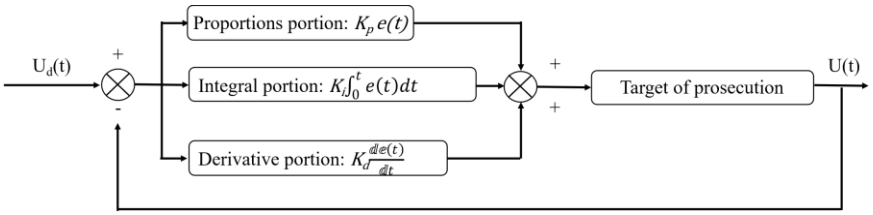

Fig.7. Principles of PID control

Before the superheat control experiment, the system operates under the following steady working conditions: absorber feed flow rate of 75L/h, distillation column feed flow rate at of 80L/h, generator temperature of 120℃, cooling water inlet temperature of 28℃. The performances of PID controls with target superheat degree values at 9.5 ℃ and 10.5 ℃ are shown in Fig. 8. Fig. 8(a) and Fig. 8(b) shows that under PID control, the deviations of superheat degree were −0.7°C to +0.7°C with control target of 9.5°C and −0.8°C to +0.7°C with control target of 10.5°C. Experimental results show that the conventional PID controller can maintain the superheat within a certain range, but obvious static deviation and fluctuation still exist. Therefore, fuzzy control and fuzzy PID control are introduced to suppress the

fluctuation and reduce the steady-state deviation, so as to further improve the control accuracy and stability of the system.

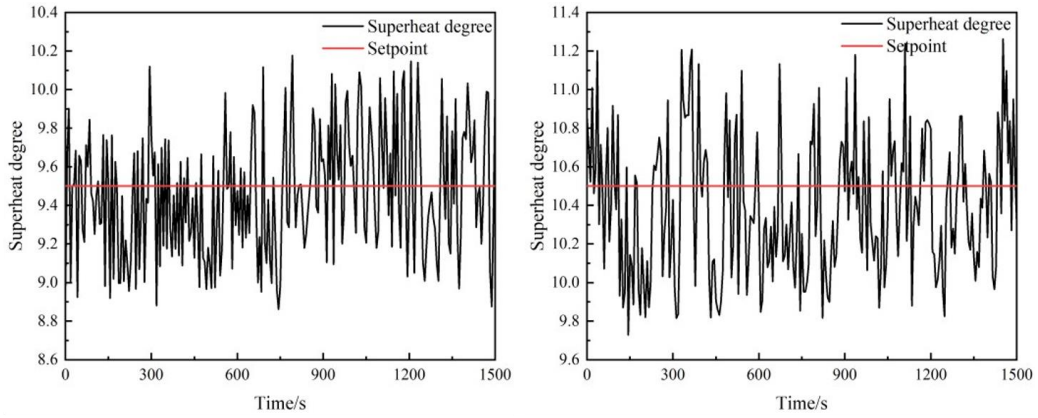

(a) Superheat degree of 9.5℃ (b) Superheat degree of 10.5℃

Fig.8. PID control curves

Although PID control has obvious limitations—the parameters of PID are fixed and lack of adaptive ability, making it difficult to cope with the nonlinear system[20]. Moreover, in many cases, the target system with PID control suffers from issues such as overshoot and oscillation[21]. These shortcomings often result in large deviation, slow response and poor stability of control[22]. Therefore, fuzzy control and fuzzy PID control are adopted in this study to improve the control performance of superheat degree.

Fuzzy control is a rule-based intelligent control method that does not rely on accurate mathematical models. The fuzzy controller uses e and e_c as inputs, and the output is the throttle device opening adjustment amount. Fuzzy subsets for e and e_c are defined as {Negative Big (NB), Negative Medium (NM), Negative Small (NS), Zero (ZO), Positive Small (PS), Positive Medium (PM), Positive Big (PB)}, and the output uses the same fuzzy subsets. According to the seven fuzzy subsets of the input variables e and e_c, a total of 49 fuzzy control rules were determined. A typical rule is as follows: if e is NB and e_c is NB, then the output is PB[23]. The principle of fuzzy control is illustrated in Fig. 9.

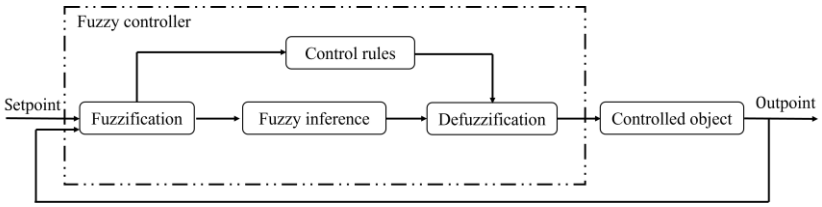

Fig.9. Principles of fuzzy control

Fuzzy PID combines the advantages of both PID and fuzzy control by online adjustment of the PID parameters: K_p, K_i, and K_d[24]. In the fuzzy PID controller, the fuzzy reasoning module takes the e and e_c as inputs, and ΔK_p, ΔK_i, and ΔK_d as outputs for the PID gains, which are used to adjust the K_p, K_i, and K_d in real time. The rule base for ΔK_p, ΔK_i, and ΔK_d is determined based on the seven fuzzy subsets (NB, NM, NS, ZO, PS, PM, PB), fuzzy control rules are similar to fuzzy control. After the real-time adjustment of K_p, K_i, and K_d by

the correction values, the new parameters serve as the input parameters of the PID controller, and the output of the PID controller is the throttle device opening adjustment amount.

The principle of fuzzy PID control is illustrated in Fig. 10.

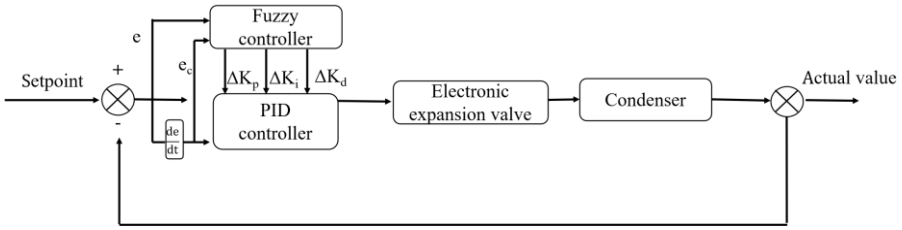

Fig.10. Principles of fuzzy PID control

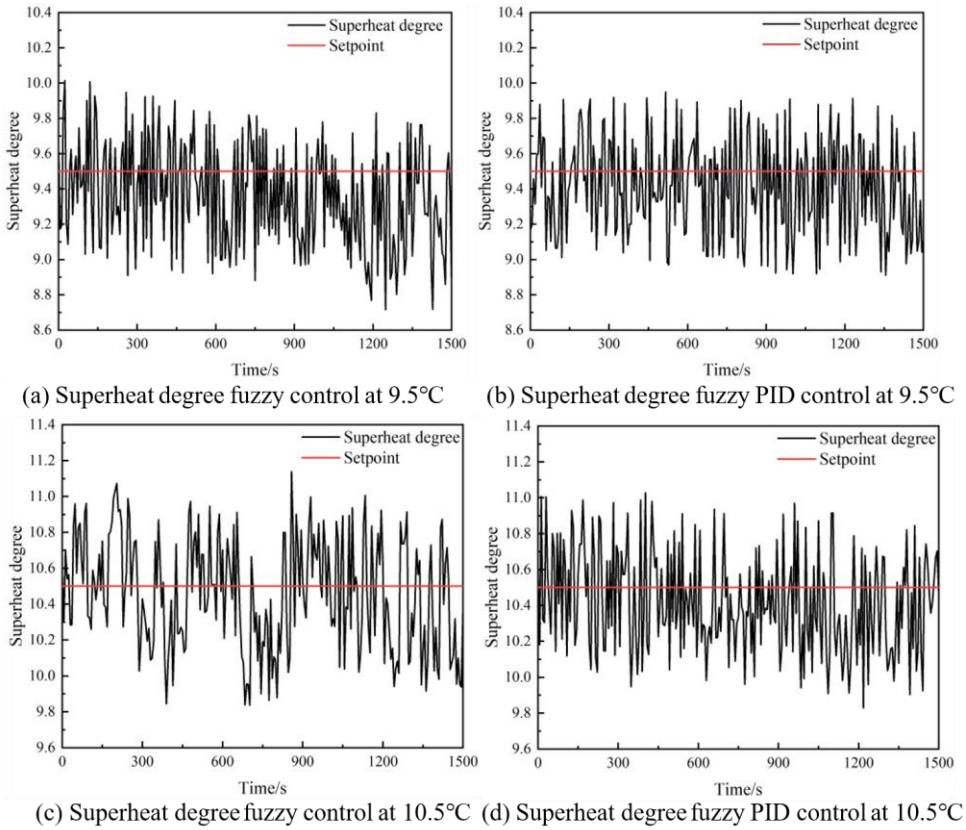

(a) Superheat degree fuzzy control at 9.5°C (b) Superheat degree fuzzy PID control at 9.5°C

(c) Superheat degree fuzzy control at 10.5°C (d) Superheat degree fuzzy PID control at 10.5°C

Fig.11. Fuzzy control and fuzzy PID control curves

The superheat control curves under fuzzy control and fuzzy PID control at setpoints of 9.5°C and 10.5°C are shown in Fig. 11. Under fuzzy control, the deviations were −1°C to +0.5°C at 9.5°C and −0.7°C to +0.6°C at 10.5°C. In contrast, fuzzy PID control further reduced the deviations to −0.6°C to +0.4°C and −0.6°C to +0.5°C, indicating improved regulation accuracy.

Standard deviation can be used to characterize data fluctuation[25]. Equation. (7) is the calculation formula for standard deviation.

$$\sigma = \sqrt{\frac{1}{n-1}\Sigma_{a=1}^{n}\left(T_{sh,a} - \bar{T}_{sh}\right)^2} \tag{7}$$

Where σ[°C], n, $T_{sh,a}$[°C], $\bar{T}_{sh}$[°C] are the standard deviation of the superheat degree,

the number of sampling points, the a-th superheat degree sampled value temperature, the average of the superheat degree temperature.

At a superheat setpoint of 9.5°C, the standard deviations were 0.32°C for PID control, 0.29°C for fuzzy control, and 0.27°C for fuzzy PID control. At 10.5°C, the corresponding values were 0.35°C, 0.31°C, and 0.27°C, respectively. Compared with PID control, fuzzy control reduced fluctuations by 10.4% and 12.8%, while compared with fuzzy control, fuzzy PID reduced standard deviation fluctuations by 7.6% and 8.8% at the two setpoints. A detailed quantitative comparison is provided in Table 4.

The results above demonstrate that the fuzzy PID controller provides the smallest deviation and lowest fluctuation among the three strategies, indicating improved temperature stability, superior steady-state accuracy of superheat degree, and potential benefits for system longevity.

Stable superheat degree helps to avoid solution concentration fluctuation and mass transfer deterioration in the absorber, thus improving operational stability of the system. However, excessive superheat degree reduces the effective heat transfer area and cooling capacity of the evaporator, while increasing the thermal load of the absorber. Therefore, an stable and accurate superheat degree control is important for the performance.

Table 4. Comparison of control performance among three algorithms

Control strategy	Superheat degree	Deviation range	Standard deviation
PID	9.5℃	(-0.7℃, +0.7℃)	0.32°C
	10.5℃	(-0.8℃, +0.7℃)	0.35°C
Fuzzy	9.5℃	(-1℃, +0.5℃)	0.29°C
	10.5℃	(-0.7℃, +0.6℃)	0.31°C
Fuzzy PID	9.5℃	(-0.6℃, +0.4℃)	0.27°C
	10.5℃	(-0.6℃, +0.5℃)	0.27°C

Step response experiments from 12.5℃ to 9.5℃ were conducted to make further comparison. The curves of three controllers are presented in Fig. 12, and the response time, overshoot, and steady-state error are compared in Table 5. Results show that, fuzzy PID achieves the fastest response, smallest undershoot, and lowest steady-state error.

Table 5. Performance comparison of three controllers under step response

Controller	Response time	Overshoot	Steady-state error
PID	280s	1℃	±0.35℃
Fuzzy	200s	0.8℃	±0.28℃

Fuzzy PID	120s	0.45℃	±0.12℃

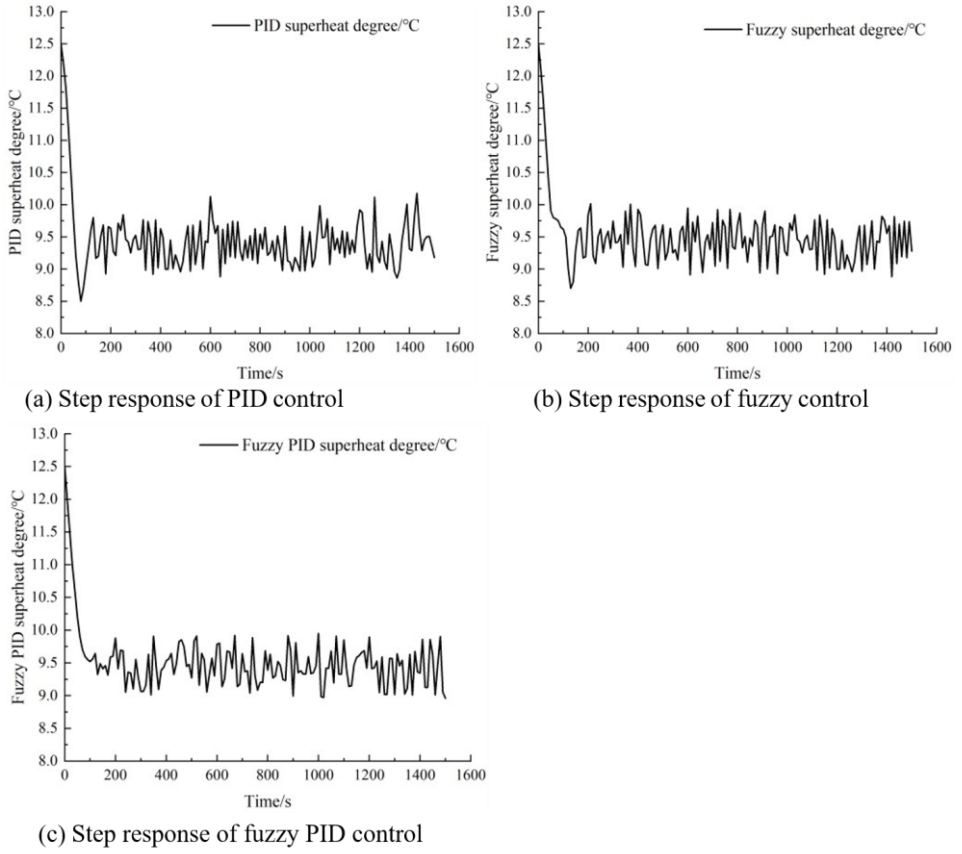

(a) Step response of PID control

(b) Step response of fuzzy control

(c) Step response of fuzzy PID control

Fig.12. Step response curve of three controllers.

4.Performance analysis of systems with different superheat degree conditions

To study the effect of the CTD on the performance of the refrigeration system, further investigations were conducted. The system performance under various superheat degree conditions was analyzed with the following parameters: absorber feed flow rate of 75L/h, distillation column feed flow rate at of 80L/h, generator temperature of 120℃, cooling water inlet temperature of 28℃ and superheat degree control algorithm using fuzzy PID.

Fig.12 illustrates the variation of evaporation temperature with increasing superheat degree. It can be observed that as superheat degree rises from 9.5°C to 13.5°C, the evaporation temperature exhibits a decreasing trend, falling from -2.7°C to -4.7°C.The reduction of the throttling valve opening decreases will result in the superheat degree increases and a decrease of the refrigerant flow, which in turn leads to the decrease of evaporation pressure and evaporation temperature.

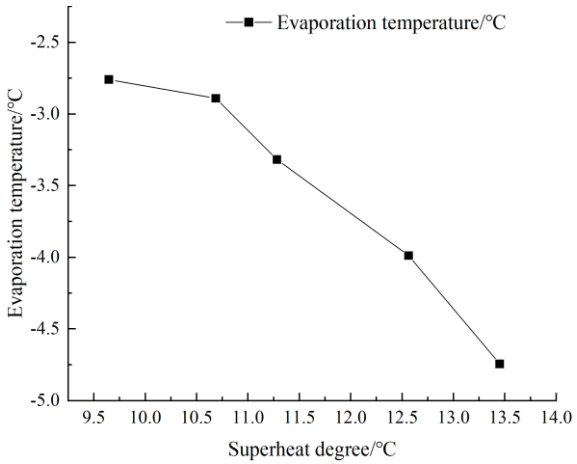

Fig.13. Evaporation temperature versus superheat degree

Fig.13 illustrates the variation curves of refrigerating capacity and COP with superheat degree. The results demonstrate that as superheat degree increases from 9.5°C to 13.5°C, both the refrigerating capacity and the COP of the system exhibit a declining trend. Specifically, refrigerating capacity decreases from 2.8 kW to 2.4 kW, while COP drops from 0.48 to 0.42.

Elevated superheat degree reduces the effective utilization of the evaporator heat transfer area and lowers the evaporator effectiveness. This results in decreased refrigerating capacity and COP. Meanwhile, the increased heat transfer temperature difference enhances irreversible losses. Moreover, an increase in the superheat degree raises the temperature of ammonia vapor entering the absorber. This not only increases the sensible heat duty of the absorber but also elevates the absorption temperature. At a fixed absorption pressure, the higher absorption temperature reduces the absorption driving force, thereby decreasing the equilibrium concentration of the rich solution at the absorber outlet.

In this study, the COP of the system is 0.48, which falls within the typical range of 0.38-0.72 reported in previous literature, but is relatively lower than some reported values under similar operating conditions. The main focus of this study is the superheat control strategy for the CTD rather than optimization of system efficiency. In addition, incomplete insulation on some connecting pipes also reduces the system COP.

To validate the effect of the proposed CTD as an alternative to EEV, performance of the system using EEV as the CTD was also tested. Result show that COP of the system using an electronic expansion valve was 0.42 with superheat degree of 9.5°C, which demonstrates the potential of the proposed CTD.

The available EEV for ammonia-water systems has a smallest rated cooling capacity of 4 kW, which is still oversized for the experimental setup, leading to a lower COP of the system. Moreover, the cost of the CTD is CNY1456, while that of the commercial EEV with controller is CNY6960. Compared to the EEV, the CTD exhibits both performance improvement and a significant financial advantage. Besides, the diverse selection of stepping motor and needle valve models enables suitable matching with refrigeration systems of various cooling capacities.

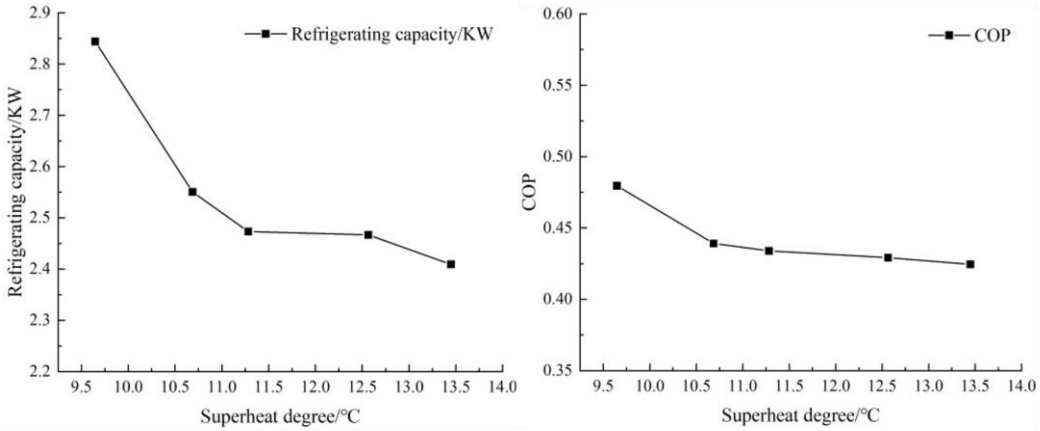

(a) Refrigerating capacity versus superheat degree (b) COP versus the superheat degree

Fig.14. Refrigerating capacity and COP versus superheat degree

5.Conclusion

In this paper, a CTD consisting of a stepper motor and a needle valve was designed as the CTD in the ammonia-water absorption refrigeration system. To validate the feasibility and the performance of the CTD, an experimental platform using PLC and LabVIEW joint control was established. The main conclusions are as follows:

(1) A low-cost, effective CTD combining a stepper motor and needle valve is proposed for the ammonia-water absorption refrigeration system. The device exhibits favorable superheat degree control performance, and the maximum deviation of the superheat degree is no more than 1°C.

(2) Fuzzy PID algorithm achieves higher control accuracy and stability than the PID or fuzzy algorithm. Fuzzy control reduces standard deviation fluctuations by 10.4% at 9.5°C and 12.8% at 10.5°C compared to PID control. While compared to fuzzy control, fuzzy PID reduces standard deviation fluctuations by 7.6% at 9.5°C and 8.8%at 10.5°C.

(3) Compared with the EEV, the system using the proposed CTD exhibits better operating performance. With the superheat degree of 9.5°C, COP of the system is 0.48, and under the same condition, COP of the system using EEV is 0.42.

(4) Long-term reliability still has to be tested under various operating conditions. And further research will be conducted on absorption system with other working fluids such as LiBr-H_2O.

Acknowledgment

This work was supported by the National Key RD Program of China (2023YFD2401304)

Nomenclature

	Symbols	out	-Outlet
Q	-Thermal power, [kW]	p	-Proportional
c	-Specific heat, [KJ $Kg^{-1}K^{-1}$]	i	-Integral
$\dot{m}$	-Mass flow rate, [kgh^{-1}]	d	-Derivative
T	-Temperature, [℃]	sh	-Superheat
$\bar{T}$	-Average temperature, [℃]		***Abbreviations***
K	-Coefficient	CTD	-Combined throttling device
ΔK	-Coefficient gain, [s]	TEV	-Thermal expansion valve
e	-Deviation	EEV	-Electronic expansion valve
e_c	-Deviation change rate	GAX	-Generator-absorber exchange
σ	-Standard deviation	SGAX	-Standard GAX
n	-Number	HEV	-Hybrid expansion valve
	Subscripts	PLC	-Programmable Logic Controller
G	-Generator	PID	-Proportional Integral Derivative
C	-Condenser	COP	-Coefficient of performance
A	-Absorber	NB	-Negative Big
R	-Refrigerating	NM	-Negative Medium
oil	-Hot oil	NS	-Negative Small
w	-Water	ZO	-Zero
chw	-Chilled water	PS	-Positive Small
cow	-Cooling water	PM	-Positive Medium
$cow1$	-Condenser cooling water	PB	-Positive Big
$cow2$	-Absorber cooling water	CNY	-Chinese Yuan
in	-Inlet		

References

[1] Kumar, M., Das, R., Experimental Analysis of Absorption Refrigeration System Driven by Waste Heat of Diesel Engine Exhaust, *Thermal Science*, *23* (2019), 1, pp. 149-157

[2] Srikhirin, P., *et al*., A Review of Absorption Refrigeration Technologies, *Renewable and Sustainable Energy Reviews*, *5* (2001), 4, pp. 343-372

[3] Ma, X., *et al*., Optimization of Zero Superheat Control at the Evaporator Outlet: Application of EXV and Pressure Regulation Valve, *Thermal Science and Engineering Progress*, *55* (2024), pp. 102919

[4] Ding, X., *et al*., A novel on-line auto-tuning PI controller for the superheat of evaporator with electronic expansion valve, *Proceedings*, *2017 Chinese Automation Congress (CAC)*, Jinan, 2017, pp. 7513-7517

[5] Shi, Y., *et al*., Thermodynamic Analysis of a Novel GAX Absorption Refrigeration Cycle, *International Journal of Hydrogen Energy*, *42* (2017), 7, pp. 4540-4547

[6] Zhao, D.D., *et al*., Theoretical Study on Solar-Driven Air-Cooled LiBr/Water Absorption Refrigeration System, *AMR*, *608-609* (2012), pp. 3-10

[7] Yari, M., *et al*., Simulation Study of the Combination of Absorption Refrigeration and Ejector-Expansion Systems, *Renewable Energy*, *60* (2013), pp. 370-381

[8] Imroz Sohel, M., Dawoud, B., Dynamic Modelling and Simulation of a Gravity-Assisted Solution Pump of a Novel Ammonia–Water Absorption Refrigeration Unit, *Applied Thermal Engineering*, *26* (2006), 7, pp. 688-699

[9] Elliott, M., *et al*., Superheat Control: A Hybrid Approach, *HVAC&R Research*, *15* (2009), 6, pp. 1021-1043

[10] Ibrahim, N., *et al*., On Dual-Loop Model-Free Adaptive Iterative Learning Control and its Application, *Journal of Process Control*, *147* (2025), pp. 103376

[11] Estrada, A., *et al*., Enhancing Vapor Compression Refrigeration Systems Efficiency Via Two-Phase Length and Superheat Evaporator MIMO Control, *Processes*, *12* (2024), 8, pp. 1600

[12] Li, S., *et al*., Design of Fractional Order PID Controller Using IMOPSOA for Degree of Superheating of Refrigerant at Evaporator Outlet, *Proceedings of the Institution of Mechanical Engineers, Part I: Journal of Systems and Control Engineering*, *239* (2025), 4, pp. 574-591

[13] Hu, H. T., *et al*., A Self-Tuning Fuzzy Logic Controller for Superheat of Evaporator by Using Electronic Expansion Valve, *Proceedings*, *2013 Sixth International Symposium on Computational Intelligence and Design*, Hangzhou, 2013, pp. 277-280

[14] Tesfay, M., *et al*., Adaptive-Model Predictive Control of Electronic Expansion Valves with Adjustable Setpoint for Evaporator Superheat Minimization, *Building and Environment*, *133* (2018), pp. 151-160

[15] Maia, A.A.T., *et al*., Superheating Control Using an Adaptive PID Controller, *HVAC&R Research*, *20* (2014), 4, pp. 424-434

[16] Elliott, M., Rasmussen, B.P., Evaporator Superheat Regulation via Emulation of Semi-Active Flow Control, *Proceedings*, *ASME 2009 Dynamic Systems and Control Conference, Volume 2*, Hollywood, California, USA, 2009, pp. 465-472

[17] Hu, Y., *et al*., Influence of Feed Flow Rate and Feed Concentration on the Ammonia Absorption Refrigeration System, *Thermal Science*, *29* (2025), 6B, pp. 4587-4598

[18] Sathyabhama, A., Ashok, B., Thermodynamic Simulation of Ammonia-Water Absorption Refrigeration System, *Thermal Science*, *12* (2008), 3, pp. 45-53
[19] Franco, S.S., *et al*., Thermal Analysis and Development of PID Control for Electronic Expansion Device of Vapor Compression Refrigeration Systems, *Applied Thermal Engineering*, *206* (2022), pp. 118130
[20] Wei, H., *et al*., Research on the Intelligent Control Strategy of Pressurizer Pressure in PWRs Based on a Fuzzy Neural Network PID Controller, *Nuclear Engineering and Design*, *433* (2025), pp. 113875
[21] Moreno, J.A., Asymptotic Tracking and Disturbance Rejection of Time-Varying Signals with a Discontinuous PID Controller, *Journal of Process Control*, *87* (2020), pp. 79-90
[22] Zhai, Y., *et al*., Intelligent PID Controller Based on Deep Reinforcement Learning, *Proceedings*, *2024 8th International Conference on Robotics*, *Control and Automation (ICRCA)*, Shanghai, 2024, pp. 343-348
[23] Dubois, D., Prade, H., What are Fuzzy Rules and How to Use them, *Fuzzy Sets and Systems*, *84* (1996), 2, pp. 169-185
[24] Zhou, Z., *et al*., Simulation analysis of steam drum water level system based on fuzzy PID control, *Proceedings*, *2024 3rd International Conference on Energy and Power Engineering, Control Engineering (EPECE)*, Chengdu, 2024, pp. 159-163
[25] Abbasi, S.A., Miller, A., MDEWMA Chart: An Efficient and Robust Alternative to Monitor Process Dispersion, *Journal of Statistical Computation and Simulation*, *83* (2013), 2, pp. 247-268

Paper submitted: 03.02.2026
Paper revised: 22.03.2026
Paper accepted: 29.03.2026